Digest Journal of Nanomaterials and Biostructures Vol.13, No.4, October-December 2018, p. 1149-1157

SYNTHESIS, CHARACTERIZATION AND PHOTOCATALYTIC PERFORMANCE INVESTIGATION OF NICKEL DOPED ZnO NANOPARTICLES

I. AHMAD[a], M. MAZHAR[a], M. N. USMANI[a,*], K. KHAN[b], S. AHMAD[c], J. AHMAD[a]

[a]*Department of Physics, Bahauddin Zakariya University, Multan. Pakistan*

[b]*Department of Electrical Engineering, The University of Azad Jammu and Kashmir, Pakistan*

[c]*Department of Building and Architectural Engineering, UCE&T, Bahauddin Zakariya University, Multan. Pakistan*

Auto-combustion method was employed to synthesize one-dimensional (1D) Zn1-xNixO (x = 0, 0.5, 0.1, 0.2, 0.3 and 0.5) nanoparticles for photocatalytic activity. XRD confirmed crystalline structure of pure and Ni-ZnO samples. Morphological and surface information of the synthesized particles was investigated by SEM. DRS results depicted that nanoparticles have direct band gap, which was reduced with Ni doping. The photoluminescence study showed that intensity was decreased with Ni concentration due to reduction of electron-hole pair rate. The influence of nickel concentration as dopant on photocatalytic behavior of Ni-ZnO was investigated. The maximum photocatalytic activity was exhibited by Ni-ZnO (x=5%) as compared to other samples.

(Received August 25, 2018; Accepted December 1, 2018)

Keywords: Nanoparticles, Auto-combustion, Photocatalytic activity, Morphology

1. Introduction

The researchers have shown great interest in nano-semiconductor photocatalysts due to their tremendous applications in overcoming environmental pollutants [1-4]. The one dimensional photocatalysts exhibit brilliant performance among the nano size materials. One aspect is larger contact surface during reactions owing to large surface area than micro scale powders, the other is easy filtration after reactions due to greater width-length ratio than other nanoparticles.

ZnO is considered to be first choice semiconductor photocatalyst among II-VI group photocatalysts due to its larger quantum efficiency than TiO2 while having almost same band gap energy (3.37eV) as that of TiO2 (3.20eV).There are many reports suggesting enhanced photocatalytic behavior of ZnO than TiO2 [5-8]. The fast recombination rate of electron-hole pair largely affects the photocatalytic behavior of ZnO and this rate is reduced by doping various ions into ZnO. Kanade et al reported that Cu doping boosted the photocatalytic behavior of ZnO nanoparticles [9]. Chang et al reported enhanced photocatalytic activity of Pd doped ZnO nanoparticles [10]. According to Qiue et al, Nitrogen doped ZnO nanoparticles have shown intensified photocatalytic activity. The morphology of photocatalyst used in their work was spherical tetrapods having size of 1um [11]. Influence of Ni concentration on photocatalytic activity of ZnO has not been discussed to date.

In this paper, we synthesized Ni doped ZnO nanoparticles with various concentrations (0.5, 0.1, 0.2, 0.3, 0.5). The structural properties of the synthesized nanoparticles are characterized by XRD. The width of optical band gap of Zn1-x NixO nano particles has been derived by taking absorption spectra. This research work has focus on a new era of one dimensional (1D) Ni-ZnO nanoparticles having approach in both fundamental research and technological applications.

*Corresponding author: naumanusmani@bzu.edu.pk

2. Experimental

2.1. Preparation of Ni-ZnO nanoparticles

All reactants were taken in original form in this research work. The auto-combustion method was used to synthesize Zn1-xNixO (x= 0%, 0.05%, 0.1%, 0.2%, 0.3%, 0.5%) nanoparticles with molar ratio Ψ = 1.7. At first, Zinc nitrate [$Zn(NO3)_2.6H2O$], Nickel nitrate [Ni(NO)3] and glycine [NH2CH2COOH] were blended in the required ratio and were placed in open air to absorb moisture, subsequently mixture was changed into paste. The paste was made homogeneous by stirring along with heat at 120˚C for one hour. On increasing temperature to 210˚C accompanied by stirring, mixture was turned into gel shape. With passage of time, gel was burst with liberation of gases. We obtained a powder after cooling to room temperature and powder was further calcinated at 700˚C for 3hours. The synthesized particles were turned into fine powder which was collected for characterization. The following chemical equation shows preparation of Ni doped ZnO nanoparticles.

$$Zn(NO_3)_2.6H_2O + Ni(NO)3 \xrightarrow{\text{Glycine}} Zn1\text{-}xNixO + \text{gaseous products}$$

2.2. Characterization techniques

Powder X-ray diffraction (XRD) was performed using computer controlled panalytical X'pert pro XRD with CuKα (λ= 1.5406nm) radiations and data was collected in a step of 0.02˚ at 2θ value ranging 20˚ to 80˚. The morphological surface and particle size was investigated by SEM (HITACHI S-4800). The DRS (λ=300-800nm) was measured by using ultraviolet-visible spectrometer (HITACHI, U-4100) along with integrating sphere accessory. The Kubelka-Munk function $F(R)\ \alpha\ K/S = (1-R^2)/2R$ was used to obtain absorbance by converting the reflectance, where K represents absorption coefficient, S, scattering coefficient and R, diffuse reflectance. The Hitachi F-4500 fluorescence spectrophotometer (λ =250-700nm) was used to record the photoluminescence (PL) spectra.

2.3. Measurement of photocatalytic activity

Photocatalytic activity of Zn1-xNixO was examined by taking 3mg of synthesized sample and dispersing it in 150ml rhodamine B aqueous solution possessing concentration of $1x10^{-5}$M. Quartz beaker accompanied by magnetic stirring was used and it took 30 min in dark to obtain the adsorption equilibrium. Ultraviolet light mercury lamp (350W) with wavelength of 365nm was used for irradiation on the dispersion. Heat effect was avoided by keeping distance of 20 cm between dispersion surface and light source.

3. Results and discussions

3.1. X-ray diffraction

The XRD patterns of pure ZnO and Ni-ZnO are shown in Fig. 1. It is clear that both have hexagonal wurtzite structure. The broad and sharp peaks (100), (002) and (101) are located at 2θ values of 31.57^0, 34.35^0 and 36.26^0 respectively. Other peaks (102) , (110) , (103) , (200) , (112) , (201) and (202) have location at 47.62^0 , 56.63^0 , 62.9^0 , 66.23^0, 68.04^0 , 69.22^0 and 77.34^0 respectively. All peaks are verified by JCPDS 05-0664 and earlier research [12]

Two specific secondary peaks (111) and (200) located at 38.42^0, 44.33^0 correspond to fcc structure of nickel as substantiated by JCPDS 04-0850 [13]. The lattice parameters for hexagonal wurtzite ZnO are a = $3.2498A^0$ and c = $5.2066A^0$ identified by JCPDS. Enhanced nickel concentration in ZnO resulted in varying diffraction peak intensity and shifting of peaks towards smaller 2θ values. The XRD pattern indicated poor crystallinity due to presence of trace quantity of unburned glycin which may be attributed to incomplete combustion reaction due to little time, moisture and carbonaceous reside in as synthesized powder [l4].

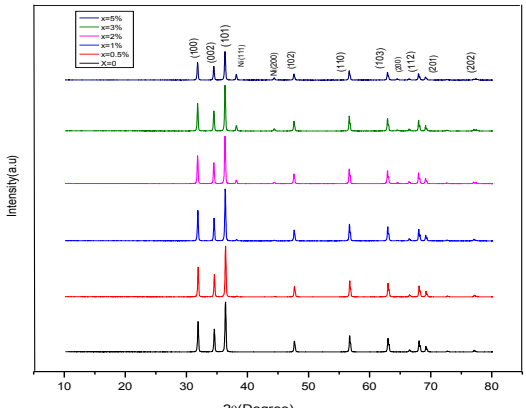

Fig. 1. XRD patterns of ZNO and Ni-ZnO.

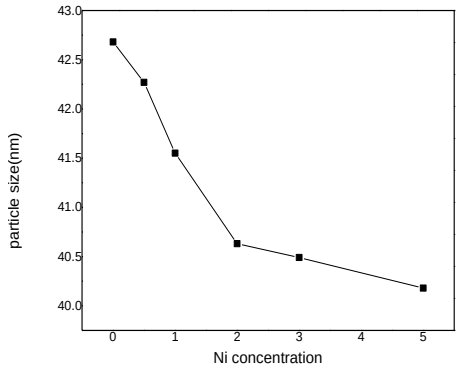

Fig. 2. Particle size Vs Ni concentration in ZnO.

The particle size was calculated by estimating full width at half maximum (FWHM) of sharp peak (101) by Scherer formula

$$D = k\lambda/\beta\cos\theta$$

Both Θ (Bragg's angle) and β (FWHM) were in radians and λ (wavelength) was in nm respectively.

When nickel was added as dopant in ZnO, particle size decreased due to Ni^{+2} substitution by Zn^{+2} into ZnO lattice and also due to Ni^{+2} incorporation to the interstitial site because of ionic radii difference of Ni^{+2} ($0.69A^0$) and Zn^{+2} ($0.74A^0$) [15]. The particles size was in range 43-40 nm.

The lattice parameters 'a' and 'c' of hexagonal wurtzite ZnO and Ni-ZnO were calculated by equation below [16].

$$1/(d_{hkl})^2 = 4/3[\ (h^2 + hk + k^2/a^2] + l^2/c^2$$

The calculated values of 'a' and 'c' for ZnO nanoparticles are a= $3.2485A^0$ and c = $5.2045A^0$ [17] and for Ni-ZnO nanoparticles (x=5%) are a=3.299 and c=3.21 respectively. Lattice strain increased the value of parameter 'a' and decreased 'c' due to ionic radii difference of Ni^{+2} ($0.69A^0$) and Zn^{+2} ($0.74A^0$). The dimension of unit cell and impact on crystal structure due to Ni^{+2} doping in ZnO lattice was determined by peak shift. Figure3 clearly indicates that peak (101) shifts towards smaller 2θ values due to ionic difference of Ni^{+2}($0.69A^0$) and Zn^{+2}($0.74A^{0)}$, showing that Ni^{+2} was substituted to Zn^{+2} successfully [18].

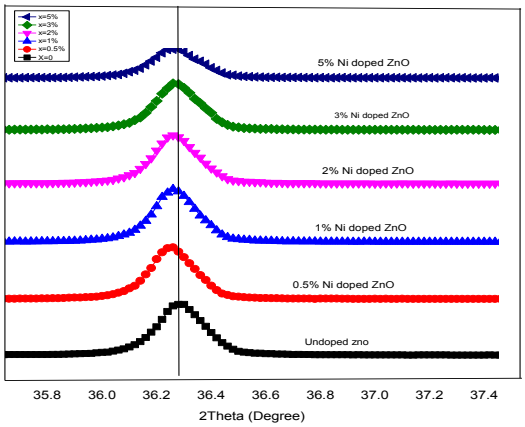

Fig. 3. Peak shift of Ni-ZnO with respect to ZnO.

Table 1. Physical parameters of ZnO and Ni-ZnO nanoparticles.

Sr. No	Samples Name	2θ at (I_{max})	FWHM = θ_1-θ_2	Crystal size from XRD (nm)	Lattice Parameters		'c/a' Ratio	Unit cell volume= $a^2cSin60^0$ $(A^0)^3$
					'a' (A^0)	'c' (A^0)		
1	Un-doped ZnO	36.32	0.3419	42.68	3.2635	3.1472	1.0369	29.0274
2	0.5% Ni doped ZnO	36.35	0.3452	42.27	3.2813	3.1993	1.0256	29.8308
3	1% Ni doped ZnO	36.36	0.3512	41.55	3.2873	3.1521	1.0427	29.4983
4	2% Ni doped ZnO	36.31	0.3591	40.63	3.2898	3.1378	1.0484	29.4091
5	3% Ni doped ZnO	36.32	0.3603	40.49	3.2915	3.1154	1.0565	29.2294
6	5% Ni doped ZnO	36.33	0.3632	40.18	3.2987	3.2067	1.0287	30.2177

3.2. Scanning electron microscopy

Fig. 4 exhibits SEM images indicating about morphology, shape and growth process of ZnO and Ni-ZnO nanoparticles. The synthesized nanoparticles are closely packed, randomly oriented and nearly spherical in shape. The density is decreased and an opposite trend is observed for porosity due to liberation of gases which rapidly decreased the surface pores and holes. With enhanced dopant concentration, the tendency of large agglomeration among smaller particles is noted. The particle size is reduced on increasing Ni concentration into ZnO which is in agreement with XRD results. Ni-ZnO (x=5%) nanoparticles showed the smallest particles size measured by ruler method [19-21].

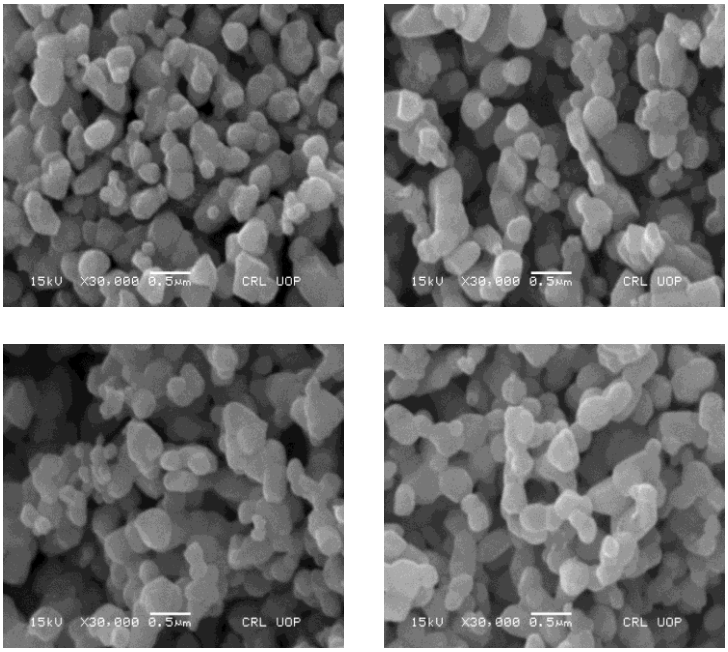

Fig. 4. SEM images for ZnO and Ni-ZnO (X=0.5%, 1%, 5%) respectively

3.3. Optical properties

3.3.1. Diffuse reflectance spectroscopy

Kubelka-Monk method was used to find the direct band gap of ZnO and Ni-ZnO nanoparticles from intersection of two linear regions by plotting absorbance Vs wavelength in range of 250-700 nm at room temperature. The specific sharp peak at 366 nm showed suppressed impurity and large crystallinity of synthesized nanoparticles. A reduction in band gap and a slight shift towards larger wavelength with increasing Ni concentration has been observed due to good interaction between oxides of Zn^{+2} and Ni^{+2} [22]. N-type carrier concentration has great role in band gap shifting and by enhancing the concentration, there occurred a red shift in band gap from UV region to visible region of electromagnetic spectrum due to interaction between d-electrons of Ni-ions and s and p-electrons of the host ZnO [23]. Also decrease in band gap was due to impurities band overlapping to conduction band [24]. Further, due to Ni^{+2} occupying the interstitial sites of ZnO lattice, reduction in direct band gap occurred due to generation of impurities band because of interaction between nickel 4d and oxygen 2p orbital, which shuffled Fermi level to valence band [25].

Table 2. Band gap of ZnO and Ni-ZnO nanoparticles.

Samples	ZnO	Ni-ZnO (x=0.05%)	Ni-ZnO (x=1%)	Ni- ZnO (x=2%)	Ni- ZnO (x=3%)	Ni- ZnO (x=5%)
Energy band gap (E= hc/λ)	3.37eV	3.34eV	3.28eV	3.21eV	3.17eV	3.08eV

The band gap of ZnO was 3.37eV and reduced to 3.08eV for Ni-ZnO (x=5%) nanoparticles due to ionic radii difference between Ni^{+2} ($0.69A^0$) and Zn^{+2} ($0.74A^0$) [26].

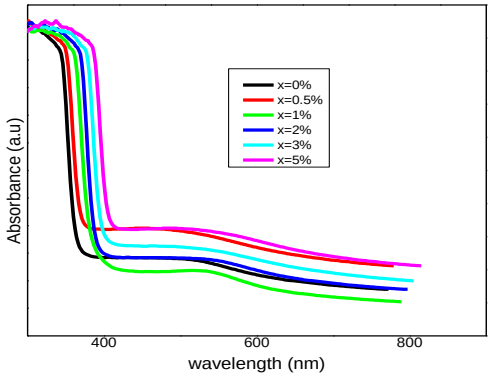

Fig. 5. UV-Vis absorption spectra.

3.3.2. Photoluminescence spectroscopy

The effect of Ni doping in ZnO lattice was investigated by PL spectroscopy at excitation wavelength of 325nm. Fig. 6 shows a plot of emission intensity and spectral content to study chemical composition, structure defects and energy transfer of synthesized samples at room temperature. The emission spectra exhibited two prominent fluorescence peaks, one at 395nm in UV region due to recombination pairs of conduction band electrons and valence band holes, second at 372nm in visible region due intrinsic and extrinsic defects [27]. Ni^{+2} doping to interstitial sites in ZnO lattice generated dual space charge and surface impurities which reduced intensity due to lower electron hole pair rate [28]. Also Ni^{+2} substituted by Zn^{+2}, generated more defects between 3d Ni^{+2} and 2p oxygen orbital and created a single acceptor state above valance band which reduced the band gap of ZnO [29]. Intensity and electron-hole recombination rate was also reduced with nickel concentration due to Ni^{+2} acting as acceptor to trap electrons [30]. A red shift in UV region was observed due to small shift in wavelength from lower photon energy to higher photon energy, which shifted Fermi level towards valence band and narrowed the band gap [31]. Among all synthesized samples, Ni-ZnO (x=5%) nanoparticles exhibited lowest intensity due to less electron hole pair rate.

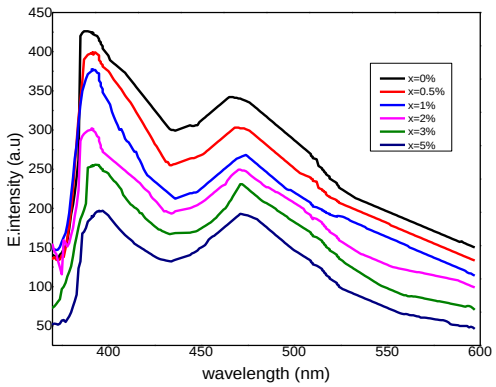

Fig. 6. Room temperature PL emission spectra of Ni-ZnO.

3.4. Photocatalytic activity

Photocatalytic activity of the synthesized Zn1-xNixO nanoparticles was investigated by using rhodamine B (RB) as photo degradation investigation [32-35]. Fig. 7 shows degradation effect of RB as photocatalyst RB using Zn1-xNixO and figure 8 demonstrates In (C0/C) versus time curves of the RB photocatalytic activity. Deep impurity levels can occur in band gap due transitional metals ions doped II-VI photocatalyst, which caused photocatalyst to absorb visible light [36-37], but there was no indication in our work for absorption in visible region of Zn1-xNixO nanoparticles as confirmed by PL spectra. Hence UV light can be used as irradiation

source. The synthesized samples of Zn1-xNixO nanoparticles were tested within 15 minutes intervals and absorption spectra gave idea about gaps between Zn1-xNixO nanoparticles. Zn1-xNixO (x=5%) nanoparticles showed best photocatalytic behavior estimated by degradation of rhodamine B (RB). These results are clear indication about positive influence on photocatalytic activity of Ni-ZnO nanoparticles in future.

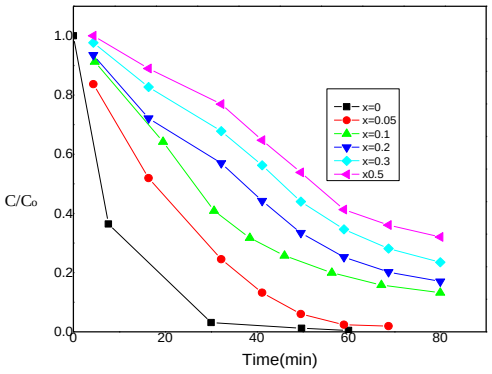

Fig. 7. Degradation effect of RB as photocatalyst RB using Zn1-xNixO.

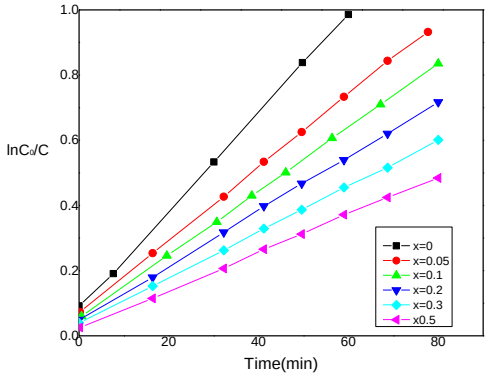

Fig. 8. In (C0/C) versus time curves of the RB photocatalytic activity.

4. Conclusion

$Zn_{1-x}Ni_xO$ (x= 0%, 0.05%, 1%, 2%, 3%, 5%) nanoparticles are synthesized by a facile auto-combustion method and investigated for photocatalytic hydrogen production. The structural properties explored by XRD confirmed hexagonal wurzite structure of prepared $Zn_{1-x}Ni_xO$ samples. Partile size decreased with Ni concentration due to ionic radii difference between Ni^{+2} and Zn^{+2}. The morphology of prepared nanoparticles was studied by SEM and tendency of large agglomeration among smaller particle was observed. PL study exhibited large effect of nickel doping on charge separation and charge recombination rate of photo induced charge carriers of ZnO. Band gap study by DRS showed that it decreases with Ni concentration. The photocatalytic performance measured by rhodamine B (RB) showed that $Zn_{1-x}Ni_xO$ (x=5%) nanoparticles have highest performances.

References

[1] K. Naeem, F. Ouyang, Physica B **405**(1), 221 (2010).
[2] Y. Xu, B. Lei, L. Guo, W. Zhou, Y. Liu, Journal of Hazardous Materials **160**(1), 78 (2008).
[3] C. Chen, W. Ma, J. Zhao, Current Organic Chemistry **14**(7), 630 (2010).
[4] H. H. Tseng, M. C. Wei, S. F. Hsiung, C. W. Chiou, Chemical Engineering Journal **150**(1), 160 009).
[5] Q. Wan, T. H. Wang, J. C. Zhao, Applied Physics Letters **87**(8), 083105 (2005).
[6] F. Xu, P. Zhang, A. Navrotsky, Z. Y. Yuan, T. Z. Ren, M. Halasa, B. L. Su, Chemistry of Materials **19**(23), 5680 (2007).
[7] C. Ye, Y. Bando, G. Shen, D. Golberg, The Journal of Physical Chemistry B, **110**(31), 15146 (2006).
[8] Y. Zheng, C. Chen, Y. Zhan, X. Lin, Q. Zheng, K. Wei, J. Zhu, The Journal of Physical Chemistry C **112**(29), 10773 (2008).
[9] K. G. Kanade, B. B. Kale, J. O. Baeg, S. M. Lee, C. W. Lee, S. J. Moon, H. Chang, Materials Chemistry and Physics **102**(1), 98 (2007).
[10] Y. Chang, J. Xu, Y. Zhang, S. Ma, L. Xin, L. Zhu, C. Xu, The Journal of Physical Chemistry C **113**(43), 18761 (2009).
[11] Y. Qiu, H. Fan, G. Tan, M. Yang, X. Yang, S. Yang, Materials Letters **131**, 64 (2014).
[12] Joint Committee on Powder Diffraction Standards (JCPDS) File No. 05-0664.
[13] P. D. File, 1967, Joint committee on powder diffraction standards. ASTM, Philadelphia, Pa, pp. 9-185.
[14] S. H. Jeong, B. N. Park, S. B. Lee, J. H. Boo, Surface and Coatings Technology **193**(1-3), 340 (2005).
[15] R. S. Zeferino, M. B. Flores, U. Pal, Journal of Applied Physics **109**(1), 014308 (2011).
[16] M. Ahmad, E. Ahmed, Y. Zhang, N. R. Khalid, J. Xu, M. Ullah, Z. Hong, Current Applied Physics **13**(4), 697 (2013).
[17] C. Karunakaran, V. Rajeswari, P. Gomathisankar, Journal of Alloys and Compounds **508**(2), 587 (2010).
[18] U. P. Gawai, H. A. Khawal, M. R. Bodke, B. N. Dole, In AIP Conference Proceedings (**1728**(1), 020607 (2016)). AIP Publishing.
[19] S. Suwanboon, Science Asia **34**(1), 31 (2008).
[20] C. C. Hwang, T. Y. Wu, Materials Science and Engineering: B **111**(2-3), 197 (2004).
[21] S. Singh, M. Arora, Nanocrystalline ZnO by Cathodic Electrochemical Deposition. In Proceedings of the Workshop on Architectural and System Support for Improving Software Dependability, New Delhi, India (pp. 501-504) 2006.
[22] U. P. Gawai, H. A. Khawal, M. R. Bodke, B. N. Dole, May. Effect of silver doping on ZnO nanocrystals. In AIP Conference Proceedings (1728(1), 020607(2016)). AIP Publishing.
[23] C. S. Lin, C. C. Hwang, W. H. Lee, W. Y. Tong, Materials Science and Engineering: B **140**(1-2), 31 (2007).
[24] T. Pauporté, O. Lupan, J. Zhang, T. Tugsuz, I. Ciofini, F. Labat, B. Viana, ACS Applied Materials & Interfaces **7**(22), 11871 (2015).
[25] F. Xu, Y. Yuan, D. Wu, M. Zhao, Z. Gao, K. Jiang, Materials Research Bulletin **48**(6), 2066 (2013).
[26] S. H. Jeong, B. N. Park, S. B. Lee, J. H. Boo, Surface and Coatings Technology **193**(1-3), 340 (2005).
[27] R. S. Zeferino, M. B. Flores, U. Pal, Journal of Applied Physics **109**(1), 014308 (2011).
[28] Y. Yan, M. M. Al-Jassim, S. H. Wei, Applied Physics Letters **89**(18), 181912 (2006).
[29] N. R. Khalid, Z. Hong, E. Ahmed, Y. Zhang, H. Chan, M. Ahmad, Applied Surface Science **258**(15), 5827 (2012).
[30] A. S. Menon, N. Kalarikkal, S. Thomas, Indian Journal of Nano Science **1**(1), 16 (2013).
[31] Q. Wan, T. H. Wang, J. C. Zhao, Applied Physics Letters **87**(8), 083105 (2005).
[32] J. Bae, J. B. Han, X. M. Zhang, M. Wei, X. Duan, Y. Zhang, Z. L. Wang, The Journal of Physical Chemistry C **113**(24), 10379 (2009).
[33] J. Wang, Z. Jiang, Z. Zhang, Y. Xie, X. Wang, Z. Xing, R. Xu, X. Zhang, Ultrasonics

Sonochemistry **15**(5), 768 (2008).
[34] J. Das, D. Khushalani, The Journal of Physical Chemistry C **114**(6), 2544 (2010).
[35] H. H. Tseng, M. C. Wei, S. F. Hsiung, C. W. Chiou, Chemical Engineering Journal **150**(1), 160009).
[36] C. Xu, L. Cao, G. Su, W. Liu, X. Qu, Y. Yu, Journal of Alloys and Compounds **497**(1-2), 373(2010).
[37] Q. Xiao, L. L. Ouyang, Journal of Alloys and Compounds **479**, L4–L7 (2009).